NEAR FIELD STUDY OF A SYNTHETIC JET

G. M. Di Cicca *, G. Iuso*, P. G. Spazzini, R. Malvano**, M. Onorato***
DIASP Politecnico di Torino, **IMGC-CNR Fluidynamics Group

Keywords: *synthetic jet, PIV*

Abstract

The analysis of an axisymmetric synthetic jet generated by an oscillating piston into a cavity has been conducted experimentally. The study has been performed in water using digital particle image velocimetry for the instantaneous velocity planar measurements. The near field and the initial part of the region where the velocity profiles start to exhibit a complete self-similarity have been investigated for two different actuation frequencies and stroke lengths. The details of the flow field have been described in terms of phase averaged flow analysis and of triple decomposition of the instantaneous velocity field. Depending on the jet flow parameters, a single vortex ring or a train of vortex rings characterizes the near field during the blowing phase.

1 Introduction

The flow field produced by a periodic oscillation of a surface under a cavity generates alternating phases of blowing and suction across an orifice or a slot [1]. Thus, momentum can be injected in the surrounding ambient although the mass flux in a period of oscillation remains equal to zero. The near field of a synthetic jet is characterized by dominant vortical structures and periodic in- and out-flow at the exit plane of the orifice. The far field, on the other hand, is characterized by a motion always directed in the downstream direction in a fashion similar to a continuous jet. In between the two fields a saddle point is present which divides streamlines directed toward the orifice and in the downstream direction.

Axisymmetric and 2D geometric configurations have been extensively studied experimentally and numerically concerning basic studies on the flow field or related with applications for flow control [4], [5], [6]. Smith and Glezer [1] focused their attention on a 2D plane turbulent synthetic jet characterized by a very high aspect ratio. They observed that each vortex of the pair develops a spanwise instability that eventually undergoes transition to turbulence, slows down, loses its coherence and becomes indistinguishable from the mean jet flow. In the far field the synthetic jet is similar to conventional 2D turbulent jets although the streamwise decrease of the mean centreline velocity of the synthetic jet is somewhat higher and the streamwise increase of its width and volume flux rate is lower. Moreover, in contrast with conventional plane jets, a synthetic jet appears to become fully turbulent closer to the exit plane.

A comparison between two dimensional flow fields generated by continuous, pulsed and synthetic jets was performed by Béra et al. [3]. The mean streamwise velocity profiles in the far field region showed good self similarity for the three different kinds of jets. The relative intensity of both velocity components fluctuations was shown to be higher for the synthetic jet with respect to the other two configurations.

Numerical simulation have also been performed to study synthetic jets in particular for planar configurations.

Kral et al. [7] presented results related with the solution of incompressible two dimensional Reynolds-Averaged Navier-Stokes equations for laminar and turbulent conditions. Comparison

of the synthetic jet computations were made with both pulsed and continuous jets assuming analytical velocity profiles at the orifice exit. Pairs of counter-rotating vortices were observed near the exit plane of the synthetic jet; at the same time the mean velocity profiles of the three jets in the far field showed a similar behavior.

An experimental and computational study was performed by Mallison et al. [9], who investigated the average flow field of a round synthetic jet in terms of velocity profiles and turbulence intensity. The flow actuator consisted in a membrane firmly clamped at its perimeter. The oscillations were achieved through a piezoeceramic disc that forced the membrane in resonant conditions. The flow attained self similarity after approximately 12 orifice diameters, i.e. well before the case of a steady jet for which self similarity is reached after 40 diameters. This behavior was explained by the turbulent dissipation, which traps a vortex near the orifice, thus limiting the size of the turbulent core.

Recently Cater and Soria [2] investigated experimentally the structure and the mean flow quantities of a round synthetic jet, generated by means of an oscillating piston into a cavity. Instantaneous velocity fields were measured by means of particle image velocimetry. They analysed the self-similarity in the far field and the radial entrainment in the near field; phase-averaged measurements were also performed.

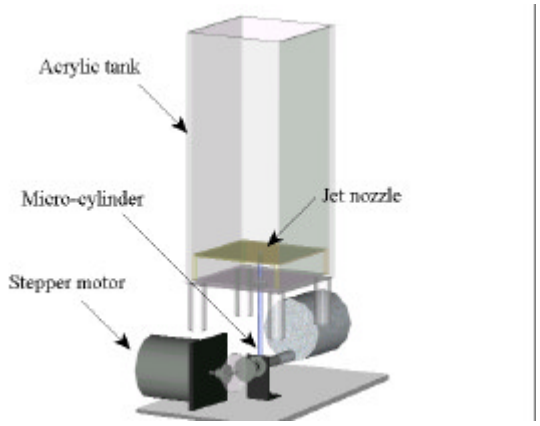

Fig. 1: Sketch of the experimental apparatus.

An exhaustive review on synthetic jets is presented by Glezer and Amitay [10]. The authors describe the evolution of an isolated synthetic jet and the physics of the interactions between a synthetic jet and a cross flow.

In the present paper the flow characteristics in the region up to x $\approx 7d_o$ of a synthetic jet are experimentally analysed for two different Reynolds numbers. Emphasis is given to the formation and the evolution of the synthetic jet.

2 Experimental Set Up and Data Reduction

Experiments were carried out in an acrylic tank 520mm deep, 255mm wide, 255mm long. The internal nozzle diameter d_0 was 7mm. The actuator system was constituted by a micro-cylinder with an internal diameter d_p of 20mm. The sinusoidal oscillation of the piston was produced by a tappet system cam mounted on a stepper motor shaft; the operating frequency ranged from 0 to 5 Hz. The eccentricity could be varied in order to modify the piston stroke while the frequency of the actuator could be changed by simply varying the step motor speed. The contraction ratio $A_R = d_p^2 / d_0^2$ of the apparatus was held constant at 8.16.

The water was seeded with spherical solid particles, 2μm nominal diameter; this dimension is small enough to allow the tracer to follow the flow faithfully. The concentration of the seeder is high enough to permit the tracking of the particle images' motion using correlation algorithms. A Nd-YAG laser source with 200mJ of energy per pulse and a duration of 8ns provided double-pulsed light sheets.

PIV measurements were taken in a (x,y) plane; x and y represent the streamwise and the radial coordinates respectively. The physical dimension of the PIV images were of 44 x 44 mm^2.

The laser beam was expanded by a cylindrical lens and focused by a spherical lens so as to form a light sheet that was approximately 0.5 mm thick. Images were recorded using a 1008 x 1012 pixels CCD videocamera Kodak Megaplus ES 1.0. The camera lens had a focal length of

105mm. The local particle-image displacement was determined by using a cross correlation based algorithm proposed by Adrian et al. [12] and Willert et al. [13], structured as an iterative multigrid method [14]. The image analysis started with an interrogation area of 64x64 pixels and the vector field obtained at this step was used for appropriately shifting the interrogation windows during the successive analysis at 32x32 pixels, providing a spatial resolution of 0.625 mm x 0.625 mm. In the last iteration the interrogation cells were 50% overlapped.

3 Results and Discussion

Measurements were carried out for two different cases. Case 1 refers to measurements taken for an oscillation frequency of 3Hz (corresponding to a period T=333ms) and a piston stroke equal to 20mm. The Reynolds number based on the mean centerline velocity at the exit section, defined by $U_0 = \frac{1}{T}\int_0^{T/2} u_0(t)dt$, and on the nozzle diameter d_o, is equal to 6860. The nondimensional stroke length L_o/d_o is equal to 46.6, where $L_0 = \int_0^{T/2} u_0(t)dt$. Case 2 refers to measurements taken at a much lower frequency and piston stroke. In particular, the oscillation frequency is 0.78Hz (corresponding to a period T=1280ms) and the piston stroke is 7.5mm. The Reynolds number is 668 and the nondimensional stroke length L_o/d_o is equal to 8.74.

Fig.2 reports an example of instantaneous velocity vector map for the case 1. For this particular instant the near flow field is characterized by a vortex ring formed at the nozzle exit and developing downstream.

Plots in fig.3a and 3b show the mean longitudinal velocity profiles, as functions of the radial distance y, at different distances from the jet exit plane, in the region up to about $2d_0$. Velocity and radial distance are made dimensionless using the centreline velocity at each distance from the nozzle and the radial distance where the velocity is half the value on the jet axis. These plots also show, for distances $x/d_o<1$, regions of negative longitudinal velocity due to the presence of vortical motions generated at the nozzle exit during the blowing phase. These peaks of negative velocity are also present for the case 2 but are much less intense than in the case 1. For $x/d_o<2$ each velocity profile exhibits a flat behavior around the jet centreline, thus evidencing the presence of a potential core, typical of continuous jets near the exit plane.

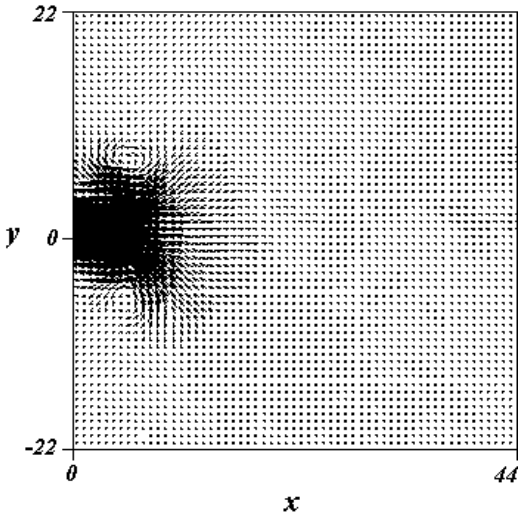

Fig.2 Instantaneous vector velocity map. Dimensions in millimeters. Case 1.

In fig.4a and 4b the mean velocity profiles are represented for $3.8d_0<x<6d_0$. It can be seen that in this range a complete self similarity characterizes the velocity profiles for the case 1. It has to be observed that self similarity for the present synthetic jet appears to be reached already at about four jet nozzle diameters downstream the exit, well before the distance at which a turbulent continuous jet becomes self similar (typically $40d_0$). This distance is also much lower with respect to values reported in bibliography: actually Mallison et al. [9], for a round jet, give a value equal to $12d_o$, nearly the same value reported by Cater and Soria [2]. In case 2, i.e. for lower oscillation frequency and piston stroke, the self similarity does not seem to be fully reached, at least in the region closer to the jet exit.

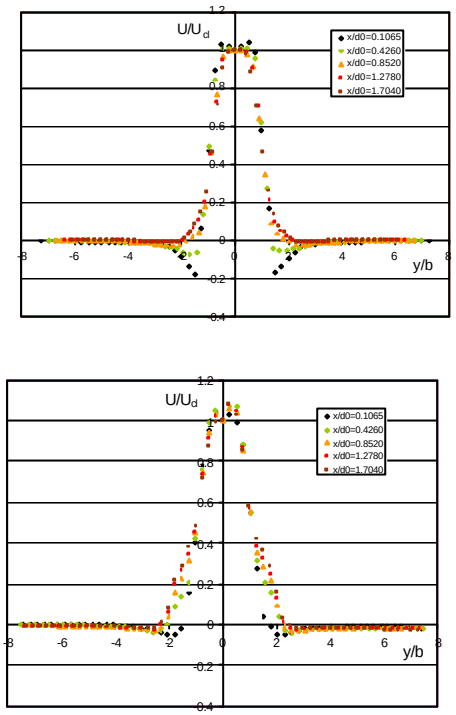

Fig.3 Nondimensional mean velocity profiles in the near field for $x/d_o<2$. a) Case 1, *f=3Hz, C=20mm, Re_{d_o}=6860, L_o/d_o=46.6*; b) Case 2, *f=0.78Hz, C=7.5mm, Re_{d_o}=668, L_o/d_o=8.74*

In 1998, Gharib, Rambod and Shariff [15] studied experimentally the formation of vortex rings generated through impulsively started jets. They experimented a wide range of piston stroke to diameter (L/D) ratios. Their results indicate that the flow field generated by large L/D consists of a leading vortex ring followed by a trailing jet. Conversely, flow fields generated by small stroke ratios show only a single vortex ring. The transition between these two distinct states occurs at a stroke ratio of approximately 4, which is called "formation number". Also, they found that the maximum circulation that a vortex ring can attain during its formation is reached at this non-dimensional formation number.

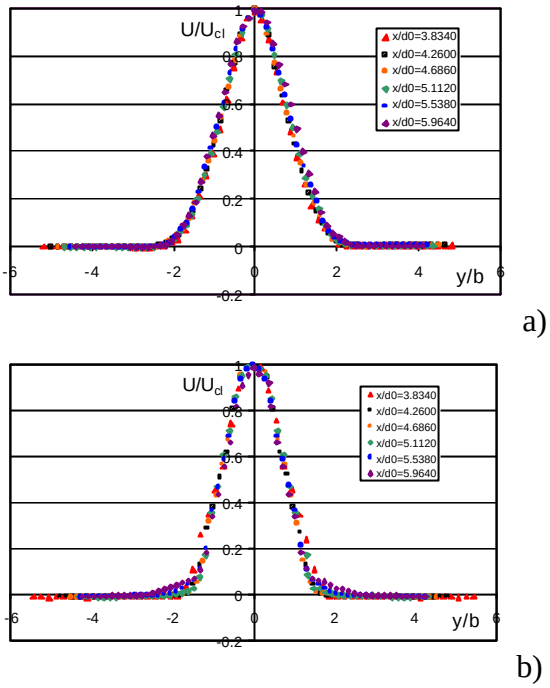

Fig.4 Nondimensional mean velocity profiles for $x/d_0>3$. a) Case 1, *f=3Hz, C=20mm, Re_{d_o}=6860, L_o/d_o=46.6*; b) Case 2, *f=0.78Hz, C=7.5mm, Re_{d_o}=668, L_o/d_o=8.74*

A similar situation can be found during the blowing phase of a synthetic jet. In figures 5a and 5b two instantaneous vector fields are represented for case 1 and case 2 respectively. The colour maps represent the vortex identification function Δ. Many techniques are available in bibliography for the vortex identification. One efficient method has been proposed by Jeong & Hussain [16]. This method involves the analysis of the eigenvalues corresponding to the local velocity gradient tensor. In the present application, the 2-D form of this tensor is computed in the PIV planes. The determinant (Δ) of the characteristic equation of the velocity gradient tensor is evaluated and it bounds vortex cores when equal to zero (Δ = 0). In case 2, for a low Reynolds number and nondimensional stroke length L_0/d_0, we can see that there is only a single vortex ring, while in case 1, for an higher Reynolds number and nondimensional stroke length L_0/d_0, there is a leading vortex ring followed by a train of smaller vortical structures.

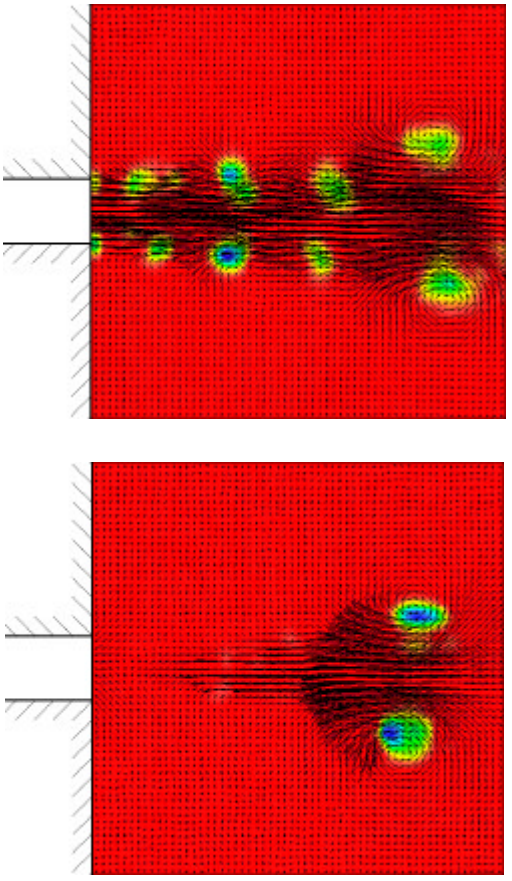

Fig.5 Near field jet evolution. a) Case 1, *f=3Hz, C=20mm, Red$_o$=6860, L$_o$/d$_o$=46.6*; b) Case 2, *f=0.78Hz, C=7.5mm, Red$_o$=668, L$_o$/d$_o$=8.74*

According to the two situations showed before, we can observe different jet behaviors. The nondimensional jet half width b/d$_o$ is displayed in fig.6 as a function of the distance from the orifice. For both cases two regions, each of them characterized by an almost constant spreading rate db/dx, are clearly identifiable. In case 1 the first region, extending up to x/d$_o$=3, is related to the near field including the saddle point. The growth rate db/dx in this zone is equal to 0.017. The second region takes place from x/d$_o$≈3 and goes on up to the last measurement section in the flow field, hence involving also the self similarity region. The growth rate is equal to 0.090, somewhat smaller than the spreading rate of conventional turbulent jets, which is nominally 0.1. The present result is in good agrement with what reported by James et al. [8] (db/dx=0.085), and Cater and Soria [2] (db/dx=0.096). In case 2 the spreading rate is much lower in the first region, while in the second region it is more or less the same as in case 1.

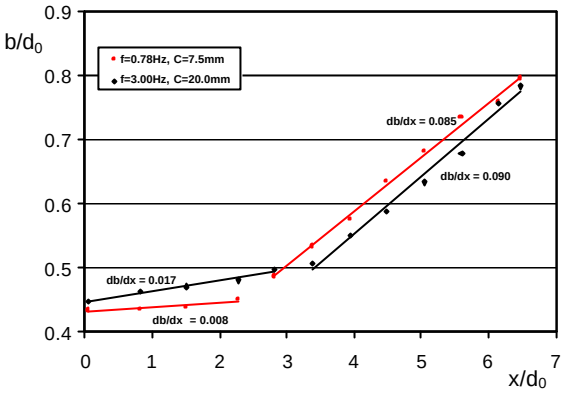

Fig.6 Jet half width evolution along the distance from the nozzle exit.

The triple decomposition proposed by Hussain and Reynolds [11] has been applied to the set of recorded images in order to describe the details of the flow field. By using this technique the flow field is decomposed in three contributions, namely the long time mean component term

$$\bar{U} = \lim_{T\to\infty} \frac{1}{T}\int_0^T U(t)\,dt$$

the coherent component

$$\tilde{u} = \langle U(t)\rangle - \bar{U}$$

and the random or incoherent component

$$u'(t) = U - \langle U(t)\rangle .$$

$\langle U(t)\rangle$ is the phase averaged part of the flow field evaluated as

$$\langle U(t)\rangle = \lim_{N\to\infty} \frac{1}{N}\sum_{n=0}^{N} U(t+nT)$$

where T is the period of the oscillation.

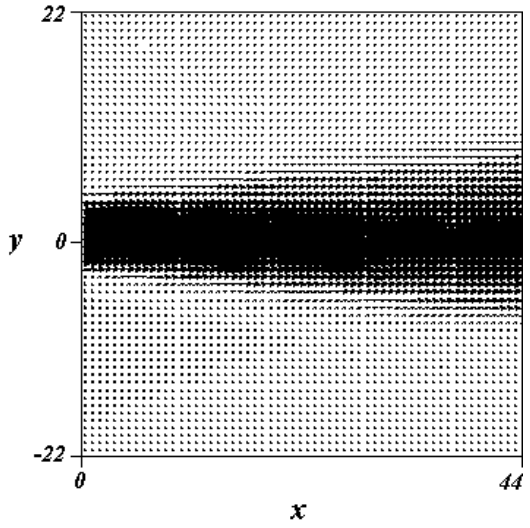

Fig.7 Mean vector velocity field. Dimensions in millimeters. Case 1

In fig.7 the mean velocity flow field calculated over 450 images, covering approximatively seven nozzle diameters along the streamwise and the radial directions, is reported for case 1. The growth rate of the synthetic jet is almost linear, as discussed before.

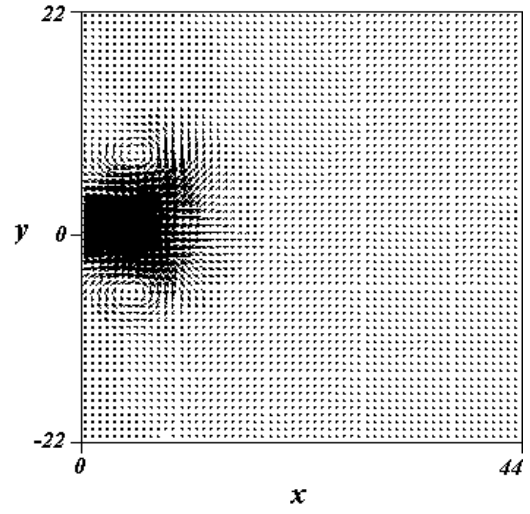

Fig. 8 Phase averaged velocity vector map for the same instant t of figure1. Dimensions in millimeters. Case 1.

Figure 8 reports the phase averaged velocity vector map computed for the same instant t as in figure 2, when the vortex ring is well formed at the nozzle exit and is being convected downstream. From the figure it is evident that the dominant structure characterizing the instantaneous flow field is a classical vortex ring.

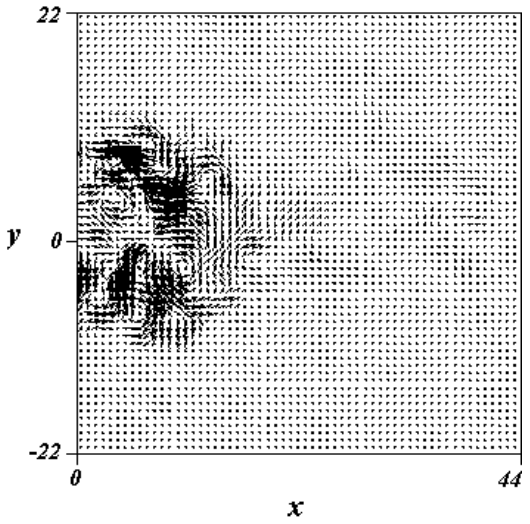

Fig.9 Random component at the same instant of figure 8. Dimensions in millimeters. Case 1.

The contribution of the random component to the total field is reported in figure 9, for the same instant corresponding to the phase averaged flow field reported in figure 8.

As it is possible to see, the incoherent contribution is characterized by random motions superimposed to small scale organized structures.

The colour map of the longitudinal velocity turbulence intensity u'_{rms}/U_{cl} , which can be put in relation with the random contribution, is reported in fig.10. The random turbulence component behaves similarly to the corresponding quantity in a continuous jet, with peaks of turbulence intensity that in the near field are shifted radially with respect to the jet axis with a significant minimum in the central portion of the flow. In the far field the peak of turbulence is located on the jet axis similarly to a steady jet. It should be noticed that these similarities cannot be observed if the periodic component $\tilde{u}$ is not taken out by means of the triple decomposition because of the strong contribution to fluctuations due to the pulsatile nature of the flow generated by the actuator.

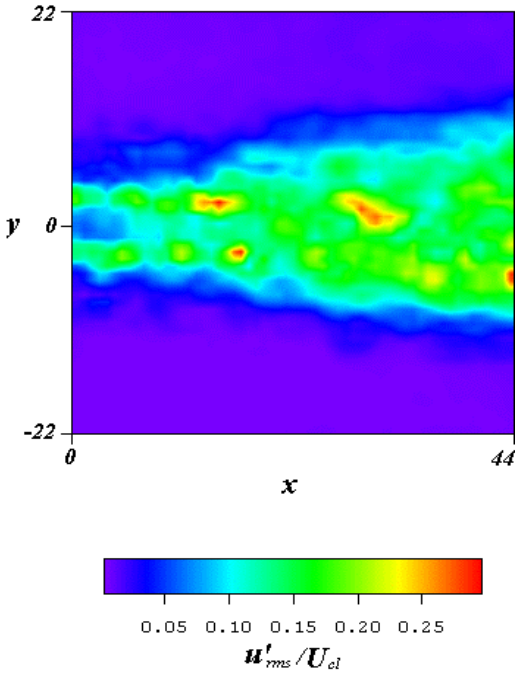

Fig. 10 Longitudinal velocity turbulence intensity. Incoherent contribution. Case 1.

4 Conclusions

The flow field of an axisymmetric synthetic jet generated by the alternating movement of a piston inside a cavity has been experimentally investigated by means of particle image velocimetry. The investigation includes the near field and the first part of the region where self similarity starts to take place.

In case 1 ($f=3Hz$, $C=20mm$, $Re_{do}=6860$, $L_o/d_o=46.6$) the mean velocity profiles exhibit a self similar behavior typical of continuous turbulent jets, for which the self similarity is reached at larger distances. In case 2 ($f=0.78Hz$, $C=7.5mm$, $Re_{do}=668$, $L_o/d_o=8.74$) self similarity does not seem to be fully reached, at least in the region of the flow field here investigated.

A single vortex ring (case 2) or a train of vortex rings (case 1) characterizes the near field during the blowing phase according to the jet flow parameters. These two different behaviors present strong analogies with the formation of vortex rings generated through impulsively started jets. Also, the two cases show different growth rates in the region closer to the nozzle exit.

References

[1] Smith B L and Glezer A The formation and evolution of synthetic jets. *Phys. Fluids* 10 (9), Sept. 1998.

[2] Cater J E and Soria J. The evolution of round zero-net-mass-flux jets. *J.Fluid Mech.*, Vol. 472, pp.167-299, 2002.

[3] Béra J C, Michard M, Grosjean N, Comte-Bellot G. Flow analysis of two-dimensional pulsed jets by particle image velocimetry. *Experiments in Fluids* 31, pp 519-532, 2001.

[4] Honohan A M, Amitay M, Glezer A. Aerodynamic control using synthetic jets. *AIAA paper 2000 – 2401*, 2000.

[5] Chen F J, Yao C, Beeler G B, Bryant R G, Fox R L Development of synthetic jet actuators for active flow control at NASA Langley. *AIAA paper 2000-2405*, 2000.

[6] Smith B L, Glezer A. Jet vectoring using synthetic jets. *J. Fluid Mech*., Vol.458, pp 1-34, 2002.

[7] Kral L D, Donovan J F, Cain A B and Cary A W. Numerical simulation of synthetic jet actuators. *AIAA Paper 97-1824*, June1997.

[8] James R D, Jacobs J W and Glezer A. A round turbulent jet produced by an oscillating diaphragm. *Phys. Fluids* 8 (9), Sept.1996.

[9] Mallison S G, Hong G and Reizes J A. Fundamental studies of a synthetic jet actuator. *13th Australian Fluid Mechanics Conference, Monash University, Melbourne, Australia*, December 1998.

[10] Glezer A and Amitay M. Synthetic jets. *Ann. Rev.Fluid Mech*., 34, pp 503-29, 2002

[11] Hussain A K M F, Reynolds W C. The mechanics of an organized wave turbulent shear flow. *J. Fluid Mech.*, Vol.41, pp 241-258, 1970.

[12] Adrian R J. Particle imaging techniques for experimental fluid mechanics. *Ann. Rev. Fluid Mech*., Vol. 23, pp 261-267, 1992.

[13] Willert C E and Gharib M. *Digital particle image velocimetry. Theory and applications.* Delft University Press, Delft, Germany, 1993.

[14] Scarano F and Riethmuller M L. Iterative multigrid approach in PIV image processing with discrete window offset. *Experiments in Fluids*, Vol. 26, pp 513-523, 1999.

[15] Gharib M, Rambod E and Shariff K A Universal Time Scale for Vortex Ring Formation. *J. Fluid Mech.*, Vol. 360, pp 121-140, 1998.

[16] Jeong J and Hussain F. On the identification of a vortex. *J. Fluid Mech.*, Vol. 285, pp 69-94, 1995.